Research Article | Vol. 29, No. 23 / 8 Nov 2021 / Optics Express 37189
Optics EXPRESS

Carbon nanotubes for polarization sensitive terahertz plasmonic interferometry

Y. Matyushkin,[1,2,3,4] S. Danilov,[2] M. Moskotin,[3,4] G. Fedorov,[3,4,7] A. Bochin,[5] I. Gorbenko,[5] V. Kachorovskii,[5,6] and S. Ganichev[2,6,8]

[1]National Research University Higher School of Economics, Moscow 101000, Russia
[2]Terahertz Center, University of Regensburg, Regensburg 93040, Germany
[3]Moscow Institute of Physics and Technology National Research University, 141700 Dolgoprudny, Russia
[4]Physics Department, Moscow Pedagogical State University (MPSU), 119435 Moscow, Russia
[5]Ioffe Institute, 194021 St. Petersburg, Russia
[6]CENTERA, Institute of High Pressure Physics PAS, 01142 Warsaw, Poland
[7]fedorov.ge@mipt.ru
[8]sergey.ganichev@physik.uni-regensburg.de

Abstract: We report on helicity sensitive photovoltaic terahertz radiation response of a carbon nanotube made in a configuration of a field-effect transistor. We find that the magnitude of the rectified voltage is different for clockwise and anticlockwise circularly polarized radiation. We demonstrate that this effect is a fingerprint of the plasma waves interference in the transistor channel. We also find that the presence of the helicity- and phase-sensitive interference part of the photovoltaic response is a universal phenomenon which is obtained in the systems of different dimensionality with different single-particle spectrum. Its magnitude is a characteristic of the plasma wave decay length. This opens up a wide avenue for applications in the area of plasmonic interferometry.

1. Introduction

Plasmonics is a rapidly growing area of research with a huge potential in terahertz photovoltaics [1,2]. In particular, plasmonic effects [3,4] were already very successfully used for robust, gate-voltage-tunable, and highly sensitive room temperature THz photodetectors based on field-effect transistors (FET), see e.g. [5–7]. Recent impressive progress in plasmonics is partially associated with appearance of novel highly-conducting carbon nanomaterials, such as graphene [6–15] and carbon nanotubes [16–18]. Record mobilities [19] observed in these materials are very promising for fabrication of plasmonic devices with high quality factors. Very recently, an extremely attractive opportunity for a further breakthrough in the area of plasmonics showed up: it has been predicted [20–23] that a conventional field-effect transistor (FET) can operate as a tunable plasmonic interferometer. This idea opens up an opportunity for applications in phase-sensitive photovoltaics. A key ingredient of a tunable plasmonic interferometer is so called phase asymmetry [22,23] that can be introduced via a simple modification to the antenna design. Such an asymmetry allows one for conversion of interfering plasma waves into dc signal due to different types of rectification effects, for example, due to hydrodynamic nonlinear phenomena. This concept was successfully implemented in our recent work [24] using a graphene-based FET. Gate-voltage-tunability, as well as the frequency- and phase- sensitivity of this graphene-based interferometer was demonstrated and successfully interpreted by using hydrodynamic approach.

Previous works [20–24] showed that a plasmonic interferometer can be realized based on 2D systems. In this paper, we show both experimentally and theoretically that quasi-one-dimensional and one-dimensional systems like carbon nanotubes which are very promising for plasmonic applications can also effectively operate as plasmonic interferometers. Our work is aimed to

#435416 https://doi.org/10.1364/OE.435416
Journal © 2021 Received 15 Jul 2021; revised 12 Sep 2021; accepted 13 Sep 2021; published 26 Oct 2021

Optics EXPRESS

demonstrate as the proof of concept possibility to realize a plasmonic interferometer using 1D conductors. We focus on fundamental study of optical excitation of plasma waves in different systems and predict a universal effect caused by plasma wave interference. In particular, response is the same (up to an irrelevant coefficient) for a single wall and multiwall CNT. We believe that this effect can be used for development of novel devices such as tunable resonant polarization-sensitive plasmonic interferometers and spectrometers as well as homodyne or heterodyne detectors based on phase-asymmetry (see Ref. [23] for discussion of such detectors in 2D systems). CNTs are advantageous for plasmon interferometry applications as compared to CVD-grown graphene because of larger momentum relaxation time. Most importantly, one can hope for the creation of interferometers operating in the regime of plasmonic resonance.

Our important experimental observation is that the magnitude of the rectified voltage for clockwise circular polarization is much smaller than that for the case of anticlockwise circularly polarized radiation. The difference between the two is larger than the response to the linearly polarized radiation. In our tilted bow-tie antenna that has an in-plane mirror axes such effect can only be explained as a manifestation of the phase sensitive interference of the plasma waves excited in the channel and plasmonic nonlinearities. We find that the presence of the helicity- and phase-sensitive interference part of the photovoltaic response is a universal phenomenon which is (up to unimportant numerical coefficients) is obtained in the systems of different dimensionality with various single particle spectrum. Also, the theory developed in this work shows plasmonic resonances which are encoded in our general formulas and can be obtained in the systems with better quality factors than ones used in our experiment. Such plasmonic resonances are gate–tunable and therefore, can be used for plasmonic interferometry.

Further development of plasmonics may be related to interferometry in more sophisticated plasmonic and polaritonic structures, similar to those described in the recent publication [25].

2. Samples and methods

Schematic cross-section of the investigated FET is shown in Fig. 1(a) and Fig. 1(c,d) shows optical photo and SEM-picture respectively. Carbon nanotubes were synthesized using chemical vapor deposition (CVD) technique with H_2 and CH_4 precursors. Catalytic nanoparticles ($Fe(NO_3)_3$; MoO_2 and Al_2O_3) were spin-coated on oxidized silicon substrate from isopropyl alcohol suspension. Such catalytic nanoparticles allow us to get single- or double- wall carbon nanotubes [26,27]. As seen from Fig. 1, there are two CNTs in our system with the following parameters: CNT1 has a length of 0.8 μm and CNT2 has a length of 2.8 μm. The diameters of both CNTs lay in the range from 2 to 4 nm. Contact interfaces to CNT and THz bow-tie antenna, were fabricated in two different parts of technological route by means of e-beam lithography and lift-off technology. CNT contact interfaces were made from Au (25 nm) by e-beam sputtering. To realize the helicity-sensitive terahertz plasmonic interferometer, the antenna sleeves were bent by 40° as shown in Fig. 1(c) and used as the source and drain electrodes. THz antennas for the radiation coupling with CNT were fabricated with thermal vacuum evaporation (Ti-Au 10-200 nm). At the final fabrication step all CNTs outside of the channel area (in the Fig. 1(d)) were etched in oxygen plasma. As seen from the Fig. 1(d), there are two nanotubes forming the conduction channel of the transistor we study in this paper. The transistor curve of this device is typical for a quasi-metallic CNT with a small band gap [28].

The silicon chip with THz radiation detector in field effect transistor configuration was anchored on an ad hoc ceramic holder. Antennas were bonded to the contact pads of the holder with a thin (25 μm) aluminum wire using an ultrasonic bonder. The holder was placed in a flow cryostat variable temperature inset. Measurements were done at a temperature of about 100 K, which is sufficiently small to exclude intensive phonon scattering and, on the other hand, is large compared to the inevitable fluctuations of the local potential due to defects in the silicon oxide and other charged impurities. For such temperature, the electron (hole) gas is degenerate at practically any

Optics EXPRESS

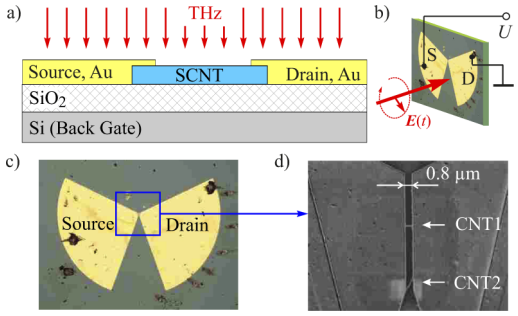

Fig. 1. Devices configuration and characterization. (a) Structures cross-section. (b) Experimental set-up. (c) and (d) Optical and scanning electron microscopy (SEM) images illustrating the device layout with source and drain electrodes connected to sleeves of a bent bow-tie antenna. The two individual CNT seen in the (d) have the lengths of 0.8 μm (upper one) and 2.8 μm (lower one). There diameters lie in the range from 2 to 4 nm.

value of the gate voltage, so that the only one type of carriers is present in the system. To obtain signals for p- and n-type free carriers and controllably vary the carrier density we used a Si back gate applying voltage V_g between Si doped substrate and drain.

The experimental set-up is sketched in Fig. 1(b). We used normally incident polarized THz radiation of a continuous wave methanol laser operating at a frequency $f = 2.54$ THz (wavelength $\lambda = 118$ μm) with a power $P \approx 20$ mW, see Refs. [29,30]. The laser spot with a diameter of about 1.5 mm was substantially larger than the device size ensuring uniform illumination of both antennas. The samples were placed in an optical cryostat and photoresponse was measured as the voltage drop U over the sample applying lock-in technique at a modulation frequency of 77 Hz. Note that due to unknown antenna efficiency we normalize the response U on the total radiation power P. The radiation polarization state was controlled by x-cut crystal quarter-wave and half-wave plates. Rotation of these plates converted initially linearly polarized laser radiation into elliptically polarized one or rotated the plane of incidence by the azimuth angle alpha, respectively. In the former case, rotation of the quarter-wave plate by and angle φ changed the radiation Stokes parameters describing the radiation helicity $P_{\rm circ}$ and the degrees of the linear polarization P_{L1} and P_{L2} after [31,32]

$$P_{\rm circ} = \sin 2\varphi\,, P_{\rm L1}(\varphi) = \frac{\cos 4\varphi + 1}{2}\,, P_{\rm L2}(\varphi) = \sin 4\varphi/2\,. \tag{1}$$

3. Results

While irradiating the device by normally incident circularly polarized radiation a photoresponse has been observed in unbiased samples. The photocurrent changes significantly if the circular polarization is switched from right-handed to left-handed circularly polarized radiation. Varying the radiation polarization state by rotating the quarter-wave plate we detected that the φ dependence of the signal is well described by

$$U = U_c P_{\rm circ} + U_{L1} P_{L1} + U_{L2} P_{L2} + U_0, \tag{2}$$

where U_c, U_{L1}, U_{L2} and U_0 are fitting parameters describing photoresponse contributions sensitive to the radiation helicity (P_c) and degrees of linear polarization (P_{L1} and P_{L2}) as well as the polarization insensitive one (U_0). The dependence is shown for $V_g = 1$ V in Fig. 2(a). In case of circularly polarized light the second and third terms in the Eq. (2) turn to zero. This, together with the fact that only the first term changes the sign by reversing the radiation helicity, makes the fitting procedure straightforward. Varying the effective gate voltage $V_g^{\rm eff} = V_g - V_g^{\rm CNP}$ results

Optics EXPRESS

in a complex behavior of the photoresponse. V_g^{CNP} is defined as the gate voltage at which the conductance of the device is minimal. We associate it with the charge neutrality point (CNP). Figure 2(b) shows the dependencies obtained for right- and left- handed circularly polarized radiation. The figure reveals that the response changes its sign at the CNP, which can naturally be attributed to the change of carrier type from positively charged holes to negatively charged electrons, and exhibits oscillations for positive gate voltages. In Fig. 3 we plotted values of the helicity sensitive (U_c) and polarization insensitive (U_0) contributions calculated based on the experimental data. These curves reveal that while at positive effective gate voltages both contributions show similar oscillatory behavior, at small negative effective gate voltages the circular response show clear oscillations, whereas both, U_0-contribution and the conductance G, shows smooth dependencies on the gate voltage.

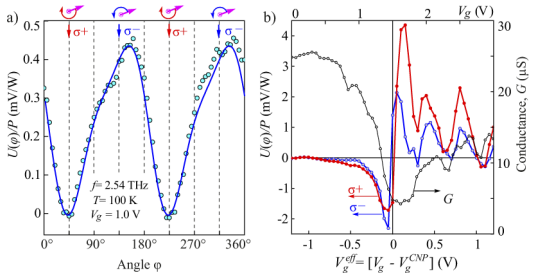

Fig. 2. (a) Helicity dependence of the photovoltage $U(\varphi)$ normalized by the laser radiation power P. Downwarded arrows labeled σ^+ and σ^- indicate angles φ corresponding to clockwise and anticlockwise rotating in-plane electric field $\boldsymbol{E}(t)$ of the right- and left-handed circularly polarized radiation, respectively. Curve is fit after Eq. (2). The ellipses on top illustrate the rotation of the electric field vector for σ^+ (φ = 45 and 225 degrees) and σ^- (φ = 135 and 315 degrees). (b) Dependencies of the photoresponse $U(\varphi)$ and the sample conductance G on the effective gate voltage $V_g^{\mathrm{eff}} = V_g - V_g^{\mathrm{CNP}}$, where V_g^{CNP} is a gate voltage corresponding to the charge neutrality point. Upper scale shows the corresponding values of the applied gate voltage V_g. Red and blue curves show responses to right- (U_{σ^+}) and left- (U_{σ^-}) handed circularly polarized radiation, respectively (see the y-axis on the left). Dashed black curve shows the sample conductance measured in the absence of THz radiation (y-axis on the right).

It is well known that the broadband rectification of terahertz radiation in a FET channel is proportional to the so-called FET factor

$$FET = G^{-1}\frac{dG}{dV_G}. \tag{3}$$

Therefore, in Fig. 3 we compared the circular response with the FET factor. We note that the $U_c(V_g)$ and $FET(V_g)$ curves have similar shapes. Both values turn to zero at the CNP and change sign at this point. Moreover, in both cases there is a decreasing trend as the gate voltage drifts away from the CNP. We also note oscillations observed for $V_g > V_g^{\mathrm{CNP}}$. It is important to understand that the oscillations in the $U_c(V_g)$ curve are not directly related to those in the $FET(V_g)$ dependence. The minima of conductance occuring to the right from the CNP may be due to irregularities of the density of states at the Fermi level [33] in an incommensurate DWNT. They should clearly somehow affect the photoresponse of our device. Still detailed analysis and understanding of these conductance and photoresposne oscillations are far beyond of the scope of this paper. This effect has recently been detected in twisted layer graphene close to the first magical angle [34].

Finally, we compared the gate dependence of the conductance measured in the dark and under irradiation with cw terahertz laser radiation (not shown). The obtained results reveal that in the

Optics EXPRESS

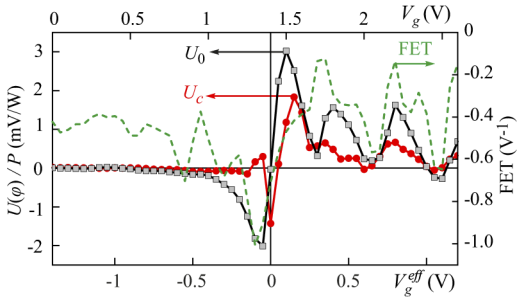

Fig. 3. Gate voltage dependencies of the circular (U_c) and polarization insensitive (U_0) photoresponse normalized on the laser laser power P. Taken into account that for the circularly polarized radiation the helicity sensitive contribution changes its sign, whereas U_0 remains unchanged and $U_{L1} = U_{L2} = 0$ (both degrees of linear polarization are zero) we calculated the amplitude after $U_c = (U_{\sigma^+} - U_{\sigma^-})/2$ and $U_0 = (U_{\sigma^+} + U_{\sigma^-})/2$. Upper scale indicates the gate voltages V_g and bottom scale indicates the corresponding effective gate voltages V_g^{eff}. Vertical line indicates the position of the CNP ($V_g^{\text{eff}} = 0$).

described experiments carried out at $T \approx 100$ K the differential conductance is not affected by the radiation, meaning that the bolometric effect [35,36] is not significant.

4. Theory

Below we present theoretical calculation of the interference contribution to dc response based on the approach used before for analysis of helicity-sensitive effects in 2D systems [22–24] with minor modifications for quasi-1D and 1D cases. We restrict ourselves to analysis of the interference helicity-sensitive contribution to dc response far from the neutrality point. We start with hydrodynamic equations describing nanotube channel far from the neutrality point, say, at the electron side of the spectrum:

$$\frac{\partial n}{\partial t} + \frac{\partial v}{\partial x} + \frac{\partial (nv)}{\partial x} = 0, \tag{4}$$

$$\frac{\partial v}{\partial t} + av\frac{\partial v}{\partial x} + \gamma(n)v = -s^2(n)\frac{\partial n}{\partial x}. \tag{5}$$

Here v is the drift velocity, $n = (N - N_F)/N_F$ is the dimensionless concentration $N = N(x, t)$ is the concentration in the channel per unit length, N_F is the equilibrium concentration, a is a coefficient on the order of unity, which we discuss below, $s^2(n) \approx s_F^2(1 - \kappa n)$, $\gamma(n) \approx \gamma_F(1 + \xi n)$ are the plasma wave velocity and damping due to the momentum relaxation, respectively. Both $s(n)$ and $\gamma(n)$ depend on the electron concentration (this dependence was neglected in Ref. [24], where plasmonic interference was studied in a 2D graphene sample). Here s_F and γ_F are their values at the Fermi level and terms $-\kappa n$ and ξn represent first order corrections with respect to n. The main difference of Eqs. (4) and 5 as compared to equations used in Refs. [22,23] for 2D electron gas with parabolic spectrum is related to different type of nonlinearities. First of all, plasma wave velocity depends on the electron concentration. Physically, this can be explained as follows. Electric force F acting on electron in the channel of the nanotube with inhomogeneous concentration leads to the following contribution to the electron acceleration $\partial v/\partial t$

$$\frac{F}{m(n)} = -\frac{e^2\Lambda}{m(n)}\frac{\partial N}{\partial x} \approx s_F^2(1 - \kappa n)\frac{\partial n}{\partial x},$$

Optics EXPRESS

where $m(n) = E(n)/v_F^2 \approx m_F(1 + \kappa n)$ is so called fictitious mass, which depends on local electron energy, E, and consequently, on the local electron concentration, $s_F^2 = e^2 N_F \ln(d/a)/m_F$ is the squared plasma wave velocity for electrons at the Fermi level [17] with $\ln(d/a)$ appearing due to $1D$ electrostatics of the problem (a and d are nanotube width and the distance to the gate, respectively). The correction to this velocity appears due to dependence of m on n. We also take into account dependence of the scattering rate on the energy and, consequently, on the electron concentration. The dimensionless factors $\kappa = m_F^{-1}(\partial m/\partial n)_{n=0}$, $\xi = \gamma_F^{-1}(\partial \gamma/\partial n)_{n=0}$ depend on the type of the nanotube (single-wall or multi-wall). Also, factor ξ depends on the type of the disorder potential.

Dependencies of s and γ on n represent two types of nonlinearities, which have not been discussed in Refs. [22–24].

The hydrodynamical term $av\partial v/\partial x$ deserves special attention. In $2D$ system with parabolic spectrum, $a = 1$. However, this is not the case for systems with linear spectrum. Moreover, a is different for a 2D system with linear spectrum, quasi-1D system, like multi-wall nanotube, and 1D system, like single-wall nanotube. As was very recently shown in Ref. [37], in 2D system with linear spectrum, $a = 0$. Specifically, in such system, the term, analogous to $v\partial v/\partial x$ for $v \ll v_F$ looks like $(v^3/2V_F^2)dv/dx$ [see Eq. (17) in Ref. [37]] and therefore can be neglected within linear-in-radiation power approximation. This result is easily extrapolated on the case of multiple 1D channels connected in parallel. In this work, we model such a quasi-1D multi-wall nanotube as a narrow strip of 2D material, i.e. assume that $a = 0$ for this case. In a full analogy with calculations of Ref. [37], one can also find for purely 1D case: $a = -1$ (we do not discuss here Luttinger liquid effects, considering nanotube within simplest semiclassical approximation based on the Boltzmann equation).

In order to compare results with the ones presented in Refs. [22,23] for parabolic spectrum, we present all equations assuming presence of term $a(vdv/dx)$ in Eq. (5) ($a = 1$ for 2D system with parabolic spectrum, $a = 0$ for multi wall nanotube, and $a = -1$ for a single wall nanotube) and for arbitrary values of a, κ and ξ.

We assume that two antennas are attached to our device, so that voltages and concentrations at the source and drain oscillate with the frequency of incoming radiation ω. Due to asymmetry of the device a phase shift θ appears between these signals. In a full analogy with Refs. [22–24] we use for the following boundary conditions for oscillating part of voltage and concentration, $n_{ac}(x = 0) = U_a \cos(\omega t + \theta)/U_g$, $n_{ac}(x = L) = U_b \cos(\omega t)/U_g$. Here U_a and U_b are the amplitudes of two phase-shifted (by phase θ) ac signals applied to the source and drain, respectively, via two antennas, and U_g is the gate potential, which controls N_F, m_F and s_F.

The general formula for response which is valid for arbitrary elliptic polarization is given in Appendix A (see Eq. (11)). Coefficients U_a and U_b entering this formula do not depend on parameters of the CNT. For a given antenna configuration these coefficients are the same as ones in the 2D case. These coefficients can be easily derived if one models antennas as two metallic rods as discussed in Ref. [24]. The nonzero dc response appears provided that these rods are rotated with respect to each other by a finite angle θ, so that antennas configuration is asymmetric. Expressions of U_a and U_b in terms of the Stokes parameters are also presented in Ref. [24]. For a more generic antenna configuration these coefficients can be used as phenomenological parameters. The phase shift, $\theta = \theta_a - \theta_b$, arises due to the tilted antennas configuration. This phase shift makes our setup asymmetrical, so it is responsible for non-zero dc response. For circularly polarized radiation the phase shift is equal to the angle between the antenna sleeves symmetry axes.

Here we only present general expression for interference contribution to the dc response, Eq. (6), which captures plasmonic resonances, and its asymptotic, Eq. (7), in the non-resonant

Optics EXPRESS

case realized in our experiment

$$U_{\text{int}} = \frac{CU_aU_b}{4U_g}\,\frac{\omega \sin\left(\frac{\Omega L}{s_F}\right)\sinh\left(\frac{\Gamma L}{s_F}\right)\sin\theta}{\sqrt{\omega^2+\gamma_F^2}\,|\sin(kL)|^2} \tag{6}$$

$$\approx \frac{CU_aU_be^{-L/L_*}\sin(L/L_*)(\omega/\gamma)\sin\theta}{U_{\text{g}}}. \tag{7}$$

where, $k = (\Omega + i\Gamma)/s_F$ is the complex wave vector of the plasma wave, and Ω, Γ obey $\Omega + i\Gamma = \sqrt{\omega(\omega + i\gamma)}$. One of the main conclusions is that this term is not very sensitive to the type of nonlinearity in the problem. Different nonlinear effects only change numerical coefficient

$$C = 4\,(1 + a - \xi)\,, \tag{8}$$

entering Eqs. (6) and 7 (we notice that κ does not enter this equation).

This implies some universality of helicity-sensitive interference response: all details of the spectrum and scattering rate are fully incorporated into a single numerical coefficient which does not depend neither from radiation frequency not from the fundamental resonant frequency of the device $\omega_0 = \pi s_F/L$. We do not focus here on exact calculation of C, which for the case of a single wall nanotube implies analysis of the Luttinger liqud effects encoded in the factor ξ. Instead, we use C as phenomenological parameter on equal footing with U_a and U_b.

Equation 6 represents general formula for the interference contribution valid for arbitrary relation between radiation frequency, plasmonic frequency $\omega_0 = \pi s_F/L$, and plasmonic damping γ_F. This equation simplifies to 7 in the non-resonant regime (and sufficiently long sample) realized in our experiment. In this case,

$\omega<\gamma_F$, $\omega_0<\gamma_F$, and $L>L_*$ where,

$$L_* = \frac{s_F\sqrt{2}}{\sqrt{\omega\gamma_F}} \tag{9}$$

is the plasma wave decay length, which we estimate for our experiment as $L_* \approx 0.2\ \mu$m.

In this regime, plasma waves, excited at the source and drain parts of the channel weakly overlap inside the transistor channel.

As was shown in Ref. [24], the response can be easily rewritten in terms of the Stokes parameters if we model two antennas attached to the source and drain by thin metallic rods of lengths R_a and R_b, respectively, rotated by angles θ_a and θ_b in the plane of the device. The circular contribution to response is equal to the interference term and is given by

$$\begin{aligned} U_{\text{circ}} = U_{\text{int}} &= \frac{U(\phi = 45^\circ) - U(\phi = 135^\circ)}{2} \\ &= -\frac{CE_0^2R_aR_b}{4U_{\text{g}}}\frac{\omega}{\gamma}\sin(L/L_*)\exp(-L/L_*)\sin(\theta_a - \theta_b), \end{aligned} \tag{10}$$

where E_0 is the amplitude of the circularly polarized wave. Since Eq. (10) contains factor $\exp(-L/L_*)$, the main contribution to gate voltage dependence of the response is due to dependence L_* on U_g.

5. Discussion of the experimental and theoretical results

The most important experimental result of this work is the observation of the helicity dependent photoresponse of the CNT based structure, see Figs. 2 and 3. So far, such a photocurrent in CNT was considered theoretically in Ref. [38] demonstrating that a response proportional to the degree of circular polarization P_{circ} is expected for chiral nanotubes. This mechanism, however,

Optics EXPRESS

cannot be responsible for the observed effect. Indeed, the helical sensitivity cannot be ascribed to the selection rules for optical transitions that lead e.g. to the optical dichroism [39] because the electromagnetic wave is not propagating along the CNT axes. Indeed, it can only be excited by radiation propagating along the CNT axis [38]. Consequently, in our experiments, applying normally incident radiation to the nanotube lying on the structure surface, it is forbidden by the symmetry arguments. Moreover, an essential part of the structure are antenna sleeves used for the radiation coupling. For elliptical (circular) radiation the antennas highly amplify a particularly oriented radiation electric field vector $\boldsymbol{E}$ so that a photoresponse is, in fact, excited by the linear polarized radiation. However, the helicity dependent signal may only results from the shifted in time excitation of the source and drain sleeves, with the phase shift different for the clockwise and anticlockwise rotating radiation $\boldsymbol{E}$, i.e. right- and left-handed circularly polarized radiation. This mechanism considered theoretically in Refs. [20–23] was most recently realized in graphene structures [24] and is caused by plasmon interference. Although we have two nanotubes in our system, one of them is "passive", since it is longer and plasma waves are much stronger decay in this nanotube (second nanotube is not grown "on purpose"). Hence, it does not contribute to the response, which is mostly determined by stronger plasma signals coming from source and drain parts of the "active" nanotube.

Now we turn to the gate dependence of the photoresponse. We begin with the sign inversion observed close to CNP. As addressed above, it is caused by the change of sign of the carrier type, and, consequently, sign inversion of the photoresponse. The photovoltage here is proportional to the first derivate of the conductance in Eq. (3) well established for the plasmonic response.

Let us compare experimental results with Eq. (10). In contrast to our previous estimates for $2D$ case [24], in 1D case both for short range of charged impurities the dependence of γ_F on energy is quite slow, and one can neglect gate voltage dependence of L_*. This conclusion agrees with our observations. Indeed, as we discussed above, interference part of the response decays with U_g approximately (see, Fig. 3) as $1/U_g$ is agreement with Eq. (10) with fixed L_*. The factor $\sin(L/L_*)/U_g$ in the Eq. (10) describes oscillations of the $U_{\rm circ}$ as a function of the gate voltage close to the CNP where the dependence of L_* on the gate voltage cannot be neglected. This may explain the experimental data shown in the Fig. 3 close to $V_g = 0$.

6. Summary

In this work, we investigated photovoltaic terahertz radiation response of a carbon nanotube electrically coupled with a gate and two antennas asymmetrically attached to source and drain. We demonstrated, both experimentally and theoretically, that response contains a large gate-controllable contribution arising due to the interference of plasma wave propagating from source and drain inside the channel. Specifically, we experimentally demonstrated that the magnitude of the rectified voltage is different for clockwise and anticlockwise circularly polarized radiation, i.e. is sensitive to the phase shift appearing as a consequence of the asymmetry of the antenna configuration. We developed a theory, which explains basic experimental results. Importantly, our theoretical analysis showed that this effect is universal in a sense that the helicity- and phase-sensitive part of the response is the same (up to unimportant numerical coefficients) in the systems of different dimensionalities with different single particle spectrum. For non-resonant regime, discussed in the current work, the magnitude of the response is fully controlled by the plasma wave decay length.

Optics EXPRESS

A. General formulas for response

Calculations, analogous to ones, presented in [22], yield the following formula for dc photoresponse

$$U_{dc} = \frac{\omega}{\sqrt{\omega^2+\gamma_F^2}} \frac{\alpha(U_a^2 - U_b^2) + \beta U_a U_b \sin\theta}{4U_g |\sin(kL)|^2} \tag{11}$$

where

$$\alpha = \left\{ \left[a + \frac{(1-\xi)\gamma_F \Omega}{\Gamma\omega} \right] - \kappa \frac{\sqrt{\omega^2+\gamma_F^2}}{\omega} \right\} \sinh^2\left(\frac{\Gamma L}{s_F}\right) + \left\{ \left[\frac{(1-\xi)\Gamma\gamma_F}{\Omega\omega} - a \right] - \kappa \frac{\sqrt{\omega^2+\gamma_F^2}}{\omega} \right\} \sin^2\left(\frac{\Omega L}{s_F}\right), \tag{12}$$

Here,

$$\beta = C \sin\left(\frac{\Omega L}{s_F}\right) \sinh\left(\frac{\Gamma L}{s_F}\right), \tag{13}$$

$k = (\Omega + i\Gamma)/s_F = \sqrt{\omega(\omega + i\gamma)}/s_F$, and $C = 4\,(1 + a - \xi)$. The term $|\sin(kL)|^2$ in denominator of Eq. (11) is responsible for plasmonic resonance. As seen, response depends on numerical coefficients a, κ and ξ. The second term in Eq. (11) is proportional to $U_a U_b$ and is responsible for the plasma wave interference effects. Different nonlinear effects only change numerical coefficient in front of this terms (in our case, coefficient 8 for 2D system with parabolic spectrum and short range scattering transforms to $4(1-\xi)$ for the linear spectrum).

Funding. FLAG-ERA Program (DeMeGRaS, GA501/16-1 of the DFG); Russian Science Foundation (20-12-00147 (theory development), 21-72-20050 (device fabrication and characterization)); Elite Network of Bavaria (K-NW-2013-247); IRAP Programme of the Foundation for Polish Science (MAB/2018/9, project CENTERA); Russian Foundation for Basic Research (21-52-12041 (device design)); Ministry of Science and Higher Education of the Russian Federation (agreement No. 075-00337-20-03, project FSMG-2020-0001 (SEM imaging)).

Disclosures. The authors declare no conflicts of interest.

Data availability. Data underlying the results presented in this paper are not publicly available at this time but may be obtained from the authors upon reasonable request.

References

1. D. Mittleman, *Sensing with terahertz radiation*, vol. 85 (Springer, 2013).
2. S. S. Dhillon, M. S. Vitiello, E. H. Linfield, A. G. Davies, M. C. Hoffmann, J. Booske, C. Paoloni, M. Gensch, P. Weightman, G. P. Williams, E. Castro-Camus, D. R. S. Cumming, F. Simoens, I. Escorcia-Carranza, J. Grant, S. Lucyszyn, M. Kuwata-Gonokami, K. Konishi, M. Koch, C. A. Schmuttenmaer, T. L. Cocker, R. Huber, A. G. Markelz, Z. D. Taylor, V. P. Wallace, J. A. Zeitler, J. Sibik, T. M. Korter, B. Ellison, S. Rea, P. Goldsmith, K. B. Cooper, R. Appleby, D. Pardo, P. G. Huggard, V. Krozer, H. Shams, M. Fice, C. Renaud, A. Seeds, A. Stöhr, M. Naftaly, N. Ridler, R. Clarke, J. E. Cunningham, and M. B. Johnston, "The 2017 terahertz science and technology roadmap," J. Phys. D: Appl. Phys. **50**(4), 043001 (2017).
3. M. Dyakonov and M. Shur, "Shallow water analogy for a ballistic field effect transistor: New mechanism of plasma wave generation by dc current," Phys. Rev. Lett. **71**(15), 2465–2468 (1993).
4. M. Dyakonov and M. Shur, "Plasma wave electronics: novel terahertz devices using two dimensional electron fluid," IEEE Trans. Electron Devices **43**(10), 1640–1645 (1996).
5. L. Vicarelli, M. S. Vitiello, D. Coquillat, A. Lombardo, A. C. Ferrari, W. Knap, M. Polini, V. Pellegrini, and A. Tredicucci, "Graphene field-effect transistors as room-temperature terahertz detectors," Nat. Mater. **11**(10), 865–871 (2012).
6. F. H. L. Koppens, T. Mueller, P. Avouris, A. C. Ferrari, M. S. Vitiello, and M. Polini, "Photodetectors based on graphene, other two-dimensional materials and hybrid systems," Nat. Nanotechnol. **9**(10), 780–793 (2014).
7. D. A. Bandurin, D. Svintsov, I. Gayduchenko, S. G. Xu, A. Principi, M. Moskotin, I. Tretyakov, D. Yagodkin, S. Zhukov, T. Taniguchi, K. Watanabe, I. V. Grigorieva, M. Polini, G. N. Goltsman, A. K. Geim, and G. Fedorov, "Resonant terahertz detection using graphene plasmons," Nat. Commun. **9**(1), 5392 (2018).

Optics EXPRESS

8. A. N. Grigorenko, M. Polini, and K. S. Novoselov, "Graphene plasmonics," Nat. Photonics **6**(11), 749–758 (2012).
9. P. D. Pietro, M. Ortolani, O. Limaj, A. D. Gaspare, V. Giliberti, F. Giorgianni, M. Brahlek, N. Bansal, N. Koirala, S. Oh, P. Calvani, and S. Lupi, "Observation of dirac plasmons in a topological insulator," Nat. Nanotechnol. **8**(8), 556–560 (2013).
10. R. R. Hartmann, J. Kono, and M. E. Portnoi, "Terahertz science and technology of carbon nanomaterials," Nanotechnology **25**(32), 322001 (2014).
11. F. Giorgianni, E. Chiadroni, A. Rovere, M. Cestelli-Guidi, A. Perucchi, M. Bellaveglia, M. Castellano, D. D. Giovenale, G. D. Pirro, M. Ferrario, R. Pompili, C. Vaccarezza, F. Villa, A. Cianchi, A. Mostacci, M. Petrarca, M. Brahlek, N. Koirala, S. Oh, and S. Lupi, "Strong nonlinear terahertz response induced by dirac surface states in bi2se3 topological insulator," Nat. Commun. **7**(1), 11421 (2016).
12. M. Autore, P. D. Pietro, A. D. Gaspare, F. D'Apuzzo, F. Giorgianni, M. Brahlek, N. Koirala, S. Oh, and S. Lupi, "Terahertz plasmonic excitations in bi2se3topological insulator," J. Phys.: Condens. Matter **29**(18), 183002 (2017).
13. A. Politano, L. Viti, and M. S. Vitiello, "Optoelectronic devices, plasmonics, and photonics with topological insulators," APL Mater. **5**(3), 035504 (2017).
14. X. Yang, Z. Sun, T. Low, H. Hu, X. Guo, F. J. G. de Abajo, P. Avouris, and Q. Dai, "Nanomaterial-based plasmon-enhanced infrared spectroscopy," Adv. Mater. **30**(20), 1704896 (2018).
15. A. Agarwal, M. S. Vitiello, L. Viti, A. Cupolillo, and A. Politano, "Plasmonics with two-dimensional semiconductors: from basic research to technological applications," Nanoscale **10**(19), 8938–8946 (2018).
16. X. He, F. Léonard, and J. Kono, "Uncooled carbon nanotube photodetectors," Adv. Opt. Mater. **3**(8), 989–1011 (2015).
17. V. Ryzhii, T. Otsuji, M. Ryzhii, V. G. Leiman, G. Fedorov, G. N. Goltzman, I. A. Gayduchenko, N. Titova, D. Coquillat, D. But, W. Knap, V. Mitin, and M. S. Shur, "Two-dimensional plasmons in lateral carbon nanotube network structures and their effect on the terahertz radiation detection," J. Appl. Phys. **120**(4), 044501 (2016).
18. R. Wang, L. Xie, S. Hameed, C. Wang, and Y. Ying, "Mechanisms and applications of carbon nanotubes in terahertz devices: A review," Carbon **132**, 42–58 (2018).
19. E. A. Laird, F. Kuemmeth, G. A. Steele, K. Grove-Rasmussen, J. Nygård, K. Flensberg, and L. P. Kouwenhoven, "Quantum transport in carbon nanotubes," Rev. Mod. Phys. **87**(3), 703–764 (2015).
20. C. Drexler, N. Dyakonova, P. Olbrich, J. Karch, M. Schafberger, K. Karpierz, Y. Mityagin, M. B. Lifshits, F. Teppe, O. Klimenko, Y. M. Meziani, W. Knap, and S. D. Ganichev, "Helicity sensitive terahertz radiation detection by field effect transistors," J. Appl. Phys. **111**(12), 124504 (2012).
21. K. S. Romanov and M. I. Dyakonov, "Theory of helicity-sensitive terahertz radiation detection by field effect transistors," Appl. Phys. Lett. **102**(15), 153502 (2013).
22. I. V. Gorbenko, V. Y. Kachorovskii, and M. S. Shur, "Plasmonic helicity-driven detector of terahertz radiation," Phys. Status Solidi RRL **13**(3), 1800464 (2019).
23. I. V. Gorbenko, V. Y. Kachorovskii, and M. Shur, "Terahertz plasmonic detector controlled by phase asymmetry," Opt. Express **27**(4), 4004 (2019).
24. Y. Matyushkin, S. Danilov, M. Moskotin, V. Belosevich, N. Kaurova, M. Rybin, E. D. Obraztsova, G. Fedorov, I. Gorbenko, V. Kachorovskii, and S. Ganichev, "Helicity-sensitive plasmonic terahertz interferometer," Nano Lett. **20**(10), 7296–7303 (2020).
25. Y. Wang, Z. Cui, X. Zhang, X. Zhang, Y. Zhu, S. Chen, and H. Hu, "Excitation of surface plasmon resonance on multiwalled carbon nanotube metasurfaces for pesticide sensors," ACS Appl. Mater. Interfaces **12**(46), 52082–52088 (2020).
26. J. Kong, H. T. Soh, A. M. Cassell, C. F. Quate, and H. Dai, "Synthesis of individual single-walled carbon nanotubes on patterned silicon wafers," Nature **395**(6705), 878–881 (1998).
27. Y. Chen, J. Huang, J. Hu, C. Yang, and W. Kang, "Synthesis of single-walled carbon nanotubes produced using a three layer al/fe/mo metal catalyst and their field emission properties," Carbon **45**(15), 3007–3014 (2007).
28. M. R. Amer, S.-W. Chang, R. Dhall, J. Qiu, and S. B. Cronin, "Zener tunneling and photocurrent generation in quasi-metallic carbon nanotube pn-devices," Nano Lett. **13**(11), 5129–5134 (2013).
29. P. Olbrich, J. Kamann, M. König, J. Munzert, L. Tutsch, J. Eroms, D. Weiss, M.-H. Liu, L. E. Golub, E. L. Ivchenko, V. V. Popov, D. V. Fateev, K. V. Mashinsky, F. Fromm, T. Seyller, and S. D. Ganichev, "Terahertz ratchet effects in graphene with a lateral superlattice," Phys. Rev. B **93**(7), 075422 (2016).
30. K.-M. Dantscher, D. A. Kozlov, M. T. Scherr, S. Gebert, J. Bärenfänger, M. V. Durnev, S. A. Tarasenko, V. V. Bel'kov, N. N. Mikhailov, S. A. Dvoretsky, Z. D. Kvon, J. Ziegler, D. Weiss, and S. D. Ganichev, "Photogalvanic probing of helical edge channels in two-dimensional HgTe topological insulators," Phys. Rev. B **95**(20), 201103 (2017).
31. V. V. Bel'kov, S. D. Ganichev, E. L. Ivchenko, S. A. Tarasenko, W. Weber, S. Giglberger, M. Olteanu, H.-P. Tranitz, S. N. Danilov, P. Schneider, W. Wegscheider, D. Weiss, and W. Prettl, "Magneto-gyrotropic photogalvanic effects in semiconductor quantum wells," J. Phys.: Condens. Matter **17**(21), 3405–3428 (2005).
32. W. Weber, L. E. Golub, S. N. Danilov, J. Karch, C. Reitmaier, B. Wittmann, V. V. Bel'kov, E. L. Ivchenko, Z. D. Kvon, N. Q. Vinh, A. F. G. van der Meer, B. Murdin, and S. D. Ganichev, "Quantum ratchet effects induced by terahertz radiation in gan-based two-dimensional structures," Phys. Rev. B **77**(24), 245304 (2008).
33. S. Wang and M. Grifoni, "Helicity and electron-correlation effects on transport properties of double-walled carbon nanotubes," Phys. Rev. Lett. **95**(26), 266802 (2005).

Optics EXPRESS

34. M. Otteneder, S. Hubmann, X. Lu, D. A. Kozlov, L. E. Golub, K. Watanabe, T. Taniguchi, D. K. Efetov, and S. D. Ganichev, "Terahertz photogalvanics in twisted bilayer graphene close to the second magic angle," Nano Lett. **20**(10), 7152–7158 (2020).
35. D. F. Santavicca, J. D. Chudow, D. E. Prober, M. S. Purewal, and P. Kim, "Bolometric and nonbolometric radio frequency detection in a metallic single-walled carbon nanotube," Appl. Phys. Lett. **98**(22), 223503 (2011).
36. J. D. Chudow, D. F. Santavicca, C. B. McKitterick, D. E. Prober, and P. Kim, "Terahertz detection mechanism and contact capacitance of individual metallic single-walled carbon nanotubes," Appl. Phys. Lett. **100**(16), 163503 (2012).
37. J. Crabb, X. Cantos-Roman, J. M. Jornet, and G. R. Aizin, "Hydrodynamic theory of the dyakonov-shur instability in graphene transistors," (2021).
38. E. L. Ivchenko and B. Spivak, "Chirality effects in carbon nanotubes," Phys. Rev. B **66**(15), 155404 (2002).
39. F. Yao, W. Yu, C. Liu, Y. Su, Y. You, H. Ma, R. Qiao, C. Wu, C. Ma, P. Gao, F. Xiao, J. Zhao, X. Bai, Z. Sun, S. Maruyama, F. Wang, J. Zhang, and K. Liu, "Complete structural characterization of single carbon nanotubes by rayleigh scattering circular dichroism,"Nature Nanotechnology (2021).